Synthesis of copper-substituted CoS2 @CuxS double-shelled nanoboxes by sequential ion exchange for efficient sodium storage

Fang, Yongjin; Luan, Deyan; Chen, Ye; Gao, Shuyan; Lou, David Xiong Wen

2020

Fang, Y., Luan, D., Chen, Y., Gao, S., & Lou, D. X. W. (2020). Synthesis of copper-substituted CoS2 @CuxS double-shelled nanoboxes by sequential ion exchange for efficient sodium storage. Angewandte Chemie International Edition, 59(7), 2644-2648. doi:10.1002/anie.201912924

https://hdl.handle.net/10356/138646

https://doi.org/10.1002/anie.201912924

Synthesis of Cu-Substituted CoS_2@Cu_xS Double-Shelled Nanoboxes via Sequential Ion Exchange for Efficient Sodium Storage

*Yongjin Fang, Deyan Luan, Ye Chen, Shuyan Gao, and Xiong Wen (David) Lou**

[*] Dr. Y. Chen, Prof. S. Y. Gao

School of Chemistry and Chemical Engineering, Henan Normal University, Xinxiang, Henan 453007, P.R. China.

Dr. Y. J. Fang, Dr. D. Y. Luan, Prof. X. W. Lou

School of Chemical and Biomedical Engineering, Nanyang Technological University, 62 Nanyang Drive, Singapore 637459, Singapore

Email: xwlou@ntu.edu.sg; davidlou88@gmail.com

Webpage: http://www.ntu.edu.sg/home/xwlou/

Abstract

Construction of hybrid architectures for electrode materials has been demonstrated as an efficient strategy to boost the sodium storage properties because of the synergetic effect from each component. However, the fabrication of hybrid nanostructures with rational structure and desired composition for decent sodium storage is still challenging. Herein, an integrated nanostructure composed of Cu-substituted CoS_2@Cu_xS double-shelled nanoboxes (denoted as Cu-CoS_2@Cu_xS DSNBs) is synthesized through a rational metal-organic framework (MOF)-based templating strategy. The unique shell configuration and complex composition endow the Cu-CoS_2@Cu_xS DSNBs with enhanced electrochemical performance in terms of superior rate capability and stable cyclability.

Keywords: MOFs, nanoboxes, CoS_2, Cu_xS, sodium-ion batteries

Because of the low cost and large reserves of sodium resources, sodium-ion batteries (SIBs) have been regarded as a promising candidate for efficient and economical energy storage.[1-6] Enormous efforts have been devoted to pursuing suitable anode materials for sodium storage, among which metal sulfides come into the spotlight in view of their high capacity and decent electrochemical reversibility.[7-9] However, most of the metal sulfides exhibit inferior rate performance and rapid capacity degradation due to the poor electric conductivity and severe volume change during sodium uptake and removal.[10, 11] Decoration by carbon species and nanostructuring are two typical efficient methods to address these issues. For example, we have synthesized hierarchical microboxes composed of carbon-coated SnS nanoplates with enhanced rate capability.[12]

Hierarchical hollow nanostructures assembled from nanosized building blocks have been reported to show boosted sodium storage properties.[13-16] The nanoscale primary units can reduce the diffusion path for both Na^+ ions and electrons, and the hollow configuration can accommodate strain during electrochemical reactions.[17] Emphatically, the integration of different active materials into one configuration has been reported to show improved physical/chemical properties with higher ionic/electric conductivity, electrochemical reactivity, and mechanical stability owing to the synergetic effects from each component.[18-22] For example, Guo and co-workers have reported the fabrication of SnS/SnO_2 heterostructures with excellent rate capability and cycling stability for SIBs.[19] On the other hand, it has been demonstrated that metal substitution can greatly improve the electrochemical properties of electrode materials in terms of capacity delivery, cyclability, and rate capability.[23, 24] For example, Co-substituted FeS_2 was reported to show enhanced cycling and rate performance.[25] Based on the aforementioned considerations, it would be of great interest by integrating these advantages into one alliance to optimize their potential for high-performance sodium storage.

Herein, a facile multistep metal-organic framework (MOF)-based templating strategy is demonstrated for preparing double-shelled nanostructures with different shell compositions, namely,

Cu-substituted CoS_2@Cu_xS double-shelled nanoboxes (denoted as Cu-CoS_2@Cu_xS DSNBs). As schematically depicted in **Figure 1**, Co-based zeolitic imidazolate framework (ZIF-67) nanocubes are first coated with Zn-based zeolitic imidazolate framework (ZIF-8) to form the ZIF-67@ZIF-8 polyhedrons through a seeded epitaxial growth process. Afterwards, the obtained ZIF-67@ZIF-8 polyhedrons are converted into CoS_2@ZnS DSNBs via a facile anion exchange process between the ZIF-67@ZIF-8 precursor and S^{2-} ions. Lastly, the CoS_2@ZnS DSNBs are further transformed into Cu-CoS_2@Cu_xS DSNBs through the cation exchange reaction with copper ions. During the cation exchange process, the inner CoS_2 layer is partly substituted with Cu^{2+} ions, whereas the outer ZnS layer is converted to Cu_xS simultaneously. Both the structure and composition of the desired Cu-CoS_2@Cu_xS DSNBs can be realized via the subtly developed recipe. Expectedly, the obtained Cu-CoS_2@Cu_xS DSNBs manifest remarkable sodium storage properties with superior rate capability and long cyclability.

ZIF-67 nanocubes synthesized via a surfactant-assisted method are adopted as the starting material. The ZIF-67 particles show a cubic shape with an average size of approximately 650 nm (**Figure 2**a and Figure S1a,b, Supporting Information (SI)). Transmission electron microscopy (TEM) images further reveal their solid nature and smooth surface (Figure 2d and Figure S1c, SI). Given that ZIF-67 and ZIF-8 are isostructural,[26, 27] a well-defined core-shell ZIF-67@ZIF-8 composite can be formed through a seeded epitaxial growth process. The obtained ZIF-67 and ZIF-67@ZIF-8 show similar X-ray diffraction (XRD) patterns (Figure S2, SI), and energy-dispersive X-ray spectroscopy (EDX) analyses (Figure S3, SI) confirm the presence of Zn element in the obtained product after the seeded epitaxial growth process. The panoramic field-emission scanning electron microscopy (FESEM) image (Figure S4a, SI) shows that the nanocube structure is well maintained. Closer FESEM examinations (Figure 2b and Figure S4b, c SI) clearly demonstrate that the edges of the nanocubes are replaced with faces, confirming the successful coating of ZIF-8 on the surface of ZIF-

67 nanocubes. The well-defined polyhedral structure of the ZIF-67@ZIF-8 particles is further confirmed by TEM studies (Figure 2e and Figure S5, SI).

We then perform the anion exchange process via the solvothermal sulfidation reaction of ZIF-67@ZIF-8 polyhedrons with a thioacetamide solution. All the diffraction peaks in the XRD pattern of the as-formed product (Figure S6a, SI) can be identified as cubic CoS_2 and cubic ZnS phases. The EDX result reveals that the CoS_2@ZnS sample holds a Co/Zn atomic ratio of about 1.49:1 (Figure S6b, SI). The polyhedral morphology is well inherited by these CoS_2@ZnS particles while the surfaces become rough (Figure 2c and Figure S7, SI). A well-defined inner cavity can be discerned unambiguously from the TEM and FESEM observations (Figure 2f, Figure S7c and S8, SI). The formation of the hollow configuration can be assigned to the diffusion-controlled ion exchange process. Specifically, at the initial stage, S^{2-} ions react with Zn^{2+} ions to form a thin layer of ZnS on the surface of ZIF-67@ZIF-8 polyhedrons, which acts as a physical barrier to hinder the chemical reaction between outside S^{2-} ions and inner Zn^{2+} and Co^{2+} ions. Owing to the smaller size of Zn^{2+} and Co^{2+} ions, the gradually outward diffusion of Zn^{2+} and Co^{2+} ions is dominant compared to the inward diffusion of S^{2-} ions. Eventually, the CoS_2@ZnS hollow particles are formed with the continuous dissolution of the ZIF-67@ZIF-8 cores and deposition of ZnS and CoS_2 on the shells.[28-30]

A cation exchange reaction is further implemented through the reaction of the as-formed CoS_2@ZnS particles with copper cations. XRD analysis reveals that the crystallographic phase of the as-derived sample can be assigned to cubic CoS_2 and hexagonal Cu_8S_5 (Figure S9a, SI). The EDX result (Figure S9b, SI) verifies the successful cation exchange process by the consequent presence of Cu signal and disappearance of Zn signal. This result is consistent with our previous study as ZnS can be completely converted to Cu_xS through a facile cation exchange reaction.[16] To further understand the reaction between the CoS_2 and copper cations, CoS_2 single-shelled nanoboxes (SSNBs) are synthesized and their reaction with Cu^{2+} cations is conducted. CoS_2 SSNBs are fabricated via the sulfidation reaction of ZIF-67 nanocubes with a thioacetamide solution (Figure S10 and S11, SI).

Then through a similar treatment in copper nitrate solution, the morphology and crystallographic phase of the CoS_2 SSNBs are maintained (Figure S12a and S13, SI). EDX analysis (Figure S12b, SI) discloses the composition of Co, Cu, and S in the structure, demonstrating the successful substitution of copper ions into the CoS_2 nanoboxes to form the Cu-substituted CoS_2 (denoted as Cu-CoS_2) SSNBs. Thus, the cation exchange reaction between Cu^{2+} cations with CoS_2@ZnS nanoboxes should give rise to the formation of Cu-substituted CoS_2@Cu_xS (Cu-CoS_2@Cu_xS).

As disclosed by FESEM and TEM images (**Figure 3**a-d and Figure S14, SI), the hollow nanobox structure is well maintained for the Cu-CoS_2@Cu_xS DSNBs after the cation exchange reaction. A closer observation of the shell of a single nanobox (Figure 3e) reveals that no noticeable intershell gap can be observed, suggesting that the Cu_xS nanoparticles are sturdily attached on the Cu-CoS_2 inner shell. A high-resolution TEM (HRTEM) image (Figure 3f) reveals the well-aligned lattice fringes with an interlayer distance of 0.27 nm, corresponding to the (1010) plane of Cu_8S_5. Elemental mapping images of a single Cu-CoS_2@Cu_xS nanobox show the even distribution of Co, Cu, and S elements in the hierarchical nanostructure (Figure 3g, h). The EDX linear scan across one Cu-CoS_2@Cu_xS nanobox demonstrates that there is a high content of Cu in the inner layer of the nanobox (Figure 3i), further proving the copper substitution into the inner CoS_2 layer as expected. And the valence states of elements in the Cu-CoS_2@Cu_xS DSNBs are determined by X-ray photoelectron spectroscopy (XPS) analysis (Figure S15, SI).

The electrochemical sodium storage behavior of the Cu-CoS_2@Cu_xS DSNBs is first studied by cyclic voltammetry (CV). The representative CV curves of the Cu-CoS_2@Cu_xS DSNBs in a voltage window of 0.4-2.6 V are shown in **Figure 4**a. During the first cathodic scan, an inconspicuous peak at 1.68 V can be ascribed to the sodium insertion into the Cu_xS,[31, 32] while the distinct peak located at 1.21 V corresponds to sodium insertion into the CoS_2.[33, 34] The broad peak at 0.8 V is assigned to the phase transformation of Na_xCuS,[35, 36] the formation of a solid electrolyte interphase (SEI) film, and the conversion reaction of Na_xCoS_2 to Co and Na_2S.[33, 37, 38] In the subsequent cathodic scans,

the main reduction peaks shift to 1.88 and 1.55 V, which are attributed to the intercalation of Na^+ ions into CuS_x and CoS_x, respectively.[36, 39-41] In the anodic scans, two peaks at about 1.86 and 2.06 V are ascribed to the reverse conversion reaction from Na_2S and Co to the CoS_x,[34, 42] while the peak at 2.16 V is assigned to the extraction of Na^+ ions from the Na_xCuS structure.[43, 44] The typical discharge-charge curves of the Cu-CoS_2@Cu_xS DSNBs at 0.1 A g^{-1} are shown in Figure 4b. Notably, a stable reversible charge capacity of about 535 mAh g^{-1} can be achieved by the Cu-CoS_2@Cu_xS DSNBs accompanied by almost overlapped discharge-charge curves from the 2nd to 5th cycles, which suggests the superb electrochemical reversibility and stability of the electrode.

Figure 4c displays the rate capability of the Cu-CoS_2@Cu_xS DSNBs cycled at various current densities. The Cu-CoS_2@Cu_xS DSNBs can deliver average capacities of 515, 446, 411, 390, 368, 349, 342 mAh g^{-1} at current densities of 0.1, 0.2, 0.3, 0.5, 1, 2, 3 A g^{-1}, respectively. In particular, even a high current density of 5 A g^{-1} is implemented, a remarkable capacity of 333 mAh g^{-1} can still be achieved. On the contrary, the capacity of the CoS_2 SSNBs drops rapidly with the increasing current density. It should be noted that the Cu-CoS_2 SSNBs exhibit much better rate performance than the CoS_2 SSNBs, indicating the facilitated electrochemical reaction via copper substitution. The discharge-charge curves at different current densities further confirm the outstanding rate capability of the Cu-CoS_2@Cu_xS DSNBs (Figure 4d). Moreover, the Cu-CoS_2@Cu_xS DSNBs electrode also exhibits a superior cycle life. Specifically, 76% of the initial capacity is preserved after 300 discharge-charge cycles at 0.3 A g^{-1} (Figure 4e). The Coulombic efficiency of the electrode steadily maintains at approximately 100% during cycling. In huge contrast, the capacity of CoS_2 SSNBs fades dramatically. The rate capability and cycling stability of Cu-CoS_2@Cu_xS DSNBs are also superior to most of the reported Co_xS-based electrodes.[34, 37, 41, 45, 46] Moreover, the nanobox structure of the Cu-CoS_2@Cu_xS DSNBs can still be well preserved after the prolonged cycling (Figure S16, SI). The outstanding electrochemical properties of these Cu-CoS_2@Cu_xS DSNBs may be ascribed to the distinctive hollow configuration and the synergistic effect of the Cu_xS nanoparticles anchored on Cu-

substituted CoS_2 nanoboxes. More specifically, the primary nanoscale building units could accelerate the reaction kinetics with shortened electron/Na^+ ion diffusion length. Both the hollow configuration and nanosized building blocks could efficiently accommodate the mechanical strain induced during the repeated discharge-charge cycling. The Cu_xS coating and Cu substitution can enhance the electric conductivity of the Cu-CoS_2@Cu_xS DSNBs so as to effectively facilitate the charge transfer process (Figure S17, SI). And the heterogeneous structure is also favorable for accelerating electron/ion transport and rendering fast kinetics.[19]

To gain some further insight into the sodium storage behavior of the Cu-CoS_2@Cu_xS DSNBs, the mechanistic investigation based on the CV test is performed. The Cu-CoS_2@Cu_xS DSNBs electrode shows well-defined redox peaks even at a high scan rate of 4.0 mV s^{-1} (**Figure 5**a). The peak current (i) and scan rate (v) obey the power law relationship: $i = av^b$, where a b value of 0.5 indicates totally diffusion-controlled electrochemical reaction, while a b value of 1.0 represents that the capacitive behavior is dominant. The b values of the four peaks are all larger than 0.75 (Figure 5b), suggesting the features of capacitive kinetics. The capacitive contributions at various scan rates can be quantified by separating the capacitive portion from the total current response at each voltage in the CV curves. For example, about 71.9% of the overall charge is capacitive at a scan rate of 2.0 mV s^{-1} based on the quantification (Figure 5c). The contribution ratios of two different components at other scan rates are also quantified (Figure 5d). The results indicate that the contribution ratio of the capacitive process gradually increases with the increasing scan rate and finally attains a maximum value of 78.3% at 4.0 mV s^{-1}. Such a high fraction of the capacitive contribution should be responsible for the superior rate capability of the Cu-CoS_2@Cu_xS DSNBs.

In summary, a multistep metal-organic framework (MOF)-based templating strategy has been designed for the rational synthesis of Cu-substituted CoS_2@Cu_xS double-shelled nanoboxes (Cu-CoS_2@Cu_xS DSNBs) for efficient sodium storage. ZIF-67@ZIF-8 polyhedrons are first synthesized via a seeded epitaxial growth process using ZIF-67 nanocubes as the starting material. Then the as-

obtained ZIF-67@ZIF-8 polyhedrons are transformed to Cu-CoS_2@Cu_xS DSNBs via the sequential ion exchange strategies by reacting with S^{2-} and Cu^{2+} ions. With the unique shell architecture and complex composition, these Cu-CoS_2@Cu_xS DSNBs exhibit boosted electrochemical sodium storage properties in terms of high capacity (535 mAh g^{-1} at 0.1 A g^{-1}), superior rate capability (333 mAh g^{-1} at 5 A g^{-1}), as well as long cyclability (76% capacity retention over 300 cycles). The work may give a spark of inspiration for the design and fabrication of complex heterostructures for various applications.

Acknowledgments

X. W. L. acknowledges the funding support from the National Research Foundation (NRF) of Singapore via the NRF investigatorship (NRF-NRFI2016-04) and Ministry of Education of Singapore via the Academic Research Fund (AcRF) Tier-1 Funding (M4011880, RG110/17).

References

[1] E. Lim, C. Jo, M. S. Kim, M.-H. Kim, J. Chun, H. Kim, J. Park, K. C. Roh, K. Kang, S. Yoon, J. Lee, *Adv. Funct. Mater.* **2016**, *26*, 3711.

[2] Y. Fang, X.-Y. Yu, X. W. Lou, *Angew. Chem. Int. Ed.* **2017**, *56*, 5801.

[3] Y. You, H.-R. Yao, S. Xin, Y.-X. Yin, T.-T. Zuo, C.-P. Yang, Y.-G. Guo, Y. Cui, L.-J. Wan, J. B. Goodenough, *Adv. Mater.* **2016**, *28*, 7243.

[4] S. Chen, C. Wu, L. Shen, C. Zhu, Y. Huang, K. Xi, J. Maier, Y. Yu, *Adv. Mater.* **2017**, *29*, 1700431.

[5] Y. Fang, Q. Liu, L. Xiao, Y. Rong, Y. Liu, Z. Chen, X. Ai, Y. Cao, H. Yang, J. Xie, C. Sun, X. Zhang, B. Aoun, X. Xing, X. Xiao, Y. Ren, *Chem* **2018**, *4*, 1167.

[6] Z. Li, X. Tan, P. Li, P. Kalisvaart, M. T. Janish, W. M. Mook, E. J. Luber, K. L. Jungjohann, C. B. Carter, D. Mitlin, *Nano Lett.* **2015**, *15*, 6339.

[7] Z. Hu, Q. Liu, S. L. Chou, S. X. Dou, *Adv. Mater.* **2017**, *29*, 1700606.

[8] J. Kim, H. Kim, K. Kang, *Adv. Energy Mater.* **2018**, *8*, 1702646.

[9] H. Pan, Y.-S. Hu, L. Chen, *Energy Environ. Sci.* **2013**, *6*, 2338.

[10] Y. Xiao, S. H. Lee, Y. K. Sun, *Adv. Energy Mater.* **2017**, *7*, 1601329.

[11] C. Fang, Y. Huang, W. Zhang, J. Han, Z. Deng, Y. Cao, H. Yang, *Adv. Energy Mater.* **2016**, *6*, 1501727.

[12] S. Wang, Y. Fang, X. Wang, X. W. Lou, *Angew. Chem. Int. Ed.* **2019**, *58*, 760.

[13] Y. Fang, X.-Y. Yu, X. W. Lou, *Adv. Mater.* **2018**, *30*, 1706668.

[14] Z. Li, Y. Fang, J. Zhang, X. W. Lou, *Adv. Mater.* **2018**, *30*, 1800525.

[15] Y. Fang, X.-Y. Yu, X. W. Lou, *Angew. Chem. Int. Ed.* **2018**, *57*, 9859.

[16] Y. Fang, X.-Y. Yu, X. W. Lou, *Angew. Chem. Int. Ed.* **2019**, *58*, 7744.

[17] F. Xie, L. Zhang, C. Ye, M. Jaroniec, S. Z. Qiao, *Adv. Mater.* **2018**, 1800492.

[18] S. Dong, C. Li, X. Ge, Z. Li, X. Miao, L. Yin, *ACS Nano* **2017**, *11*, 6474.

[19] Y. Zheng, T. Zhou, C. Zhang, J. Mao, H. Liu, Z. Guo, *Angew. Chem. Int. Ed.* **2016**, *55*, 3408.

[20] C. Yang, X. Liang, X. Ou, Q. Zhang, H.-S. Zheng, F. Zheng, J.-H. Wang, K. Huang, M. Liu, *Adv. Funct. Mater.* **2019**, *29*, 1807971.

[21] X. Y. Yu, X. W. Lou, *Adv. Energy Mater.* **2018**, *8*, 1701592.

[22] Y. Fang, B. Y. Guan, D. Luan, X. W. Lou, *Angew. Chem. Int. Ed.* **2019**, *58*, 7739.

[23] Y. Huang, M. Xie, Z. Wang, Y. Jiang, G. Xiao, S. Li, L. Li, F. Wu, R. Chen, *Energy Storage Mater.* **2018**, *11*, 100.

[24] D. D. Yuan, Y. X. Wang, Y. L. Cao, X. P. Ai, H. X. Yang, *ACS Appl. Mater. Interfaces* **2015**, *7*, 8585.

[25] K. Zhang, M. Park, L. Zhou, G. H. Lee, J. Shin, Z. Hu, S. L. Chou, J. Chen, Y. M. Kang, *Angew. Chem. Int. Ed.* **2016**, *55*, 12822.

[26] J. Yang, F. Zhang, H. Lu, X. Hong, H. Jiang, Y. Wu, Y. Li, *Angew. Chem. Int. Ed.* **2015**, *54*, 10889.

[27] G. Zhan, H. C. Zeng, *Nat. Commun.* **2018**, *9*, 3778.

[28] H. Hu, B. Y. Guan, X. W. Lou, *Chem* **2016**, *1*, 102.

[29] P. Zhang, B. Y. Guan, L. Yu, X. W. Lou, *Chem* **2018**, *4*, 162.

[30] Z. Jiang, H. Sun, Z. Qin, X. Jiao, D. Chen, *Chem. Commun.* **2012**, *48*, 3620.

[31] J.-S. Kim, D.-Y. Kim, G.-B. Cho, T.-H. Nam, K.-W. Kim, H.-S. Ryu, J.-H. Ahn, H.-J. Ahn, *J. Power Sources* **2009**, *189*, 864.

[32] Q. Chen, M. Ren, H. Xu, W. Liu, J. Hei, L. Su, L. Wang, *ChemElectroChem* **2018**, *5*, 2135.

[33] Y. Pan, X. Cheng, Y. Huang, L. Gong, H. Zhang, *ACS Appl. Mater. Interfaces* **2017**, *9*, 35820.

[34] Z. Shadike, M.-H. Cao, F. Ding, L. Sang, Z.-W. Fu, *Chem. Commun.* **2015**, *51*, 10486.

[35] C. An, Y. Ni, Z. Wang, X. Li, X. Liu, *Inorg. Chem. Front.* **2018**, *5*, 1045.

[36] Z. Yang, T. Chen, C. Wu, J. Qu, Z. Wu, X. Guo, B. Zhong, H. Liu, S. Dou, *ACS Appl. Mater. Interfaces* **2019**, *11*, 3961.

[37] Y. Xiao, J.-Y. Hwang, I. Belharouak, Y.-K. Sun, *Nano Energy* **2017**, *32*, 320.

[38] L. Zhou, K. Zhang, J. Sheng, Q. An, Z. Tao, Y.-M. Kang, J. Chen, L. Mai, *Nano Energy* **2017**, *35*, 281.

[39] J. Li, D. Yan, T. Lu, W. Qin, Y. Yao, L. Pan, *ACS Appl. Mater. Interfaces* **2017**, *9*, 2309.

[40] Y. Pan, X. Cheng, L. Gong, L. Shi, Y. Deng, H. Zhang, *J. Mater. Chem. A* **2018**, *6*, 18967.

[41] F. Han, T. Lv, B. Sun, W. Tang, C. Zhang, X. Li, *RSC Adv.* **2017**, *7*, 30699.

[42] X. Liu, K. Zhang, K. Lei, F. Li, Z. Tao, J. Chen, *Nano Res.* **2016**, *9*, 198.

[43] A. Qin, H. Wu, J. Chen, T. Li, S. Chen, D. Zhang, F. Xu, *Nanoscale* **2019**, *11*, 7188.

[44] Y. Xiao, D. Su, X. Wang, S. Wu, L. Zhou, Y. Shi, S. Fang, H. M. Cheng, F. Li, *Adv. Energy Mater.* **2018**, *8*, 1800930.

[45] X. Wang, Y. Chen, Y. Fang, J. Zhang, S. Gao, X. W. Lou, *Angew. Chem. Int. Ed.* **2019**, *58*, 2675.

[46] C. Wu, Y. Jiang, P. Kopold, P. A. van Aken, J. Maier, Y. Yu, *Adv. Mater.* **2016**, *28*, 7276.

Figures and Captions

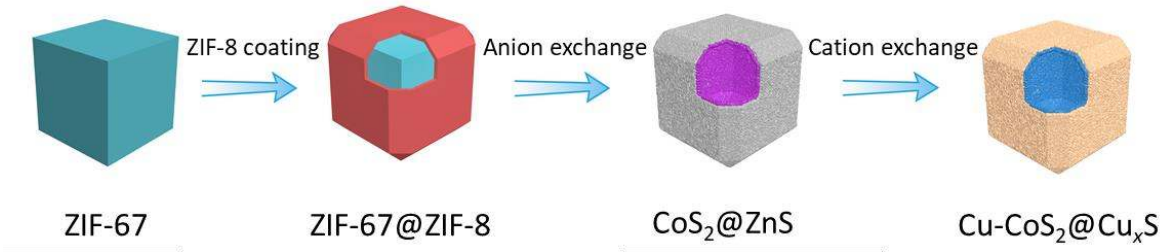

Figure 1. Schematic illustration of the synthetic process of the Cu-CoS_2@Cu_xS DSNBs.

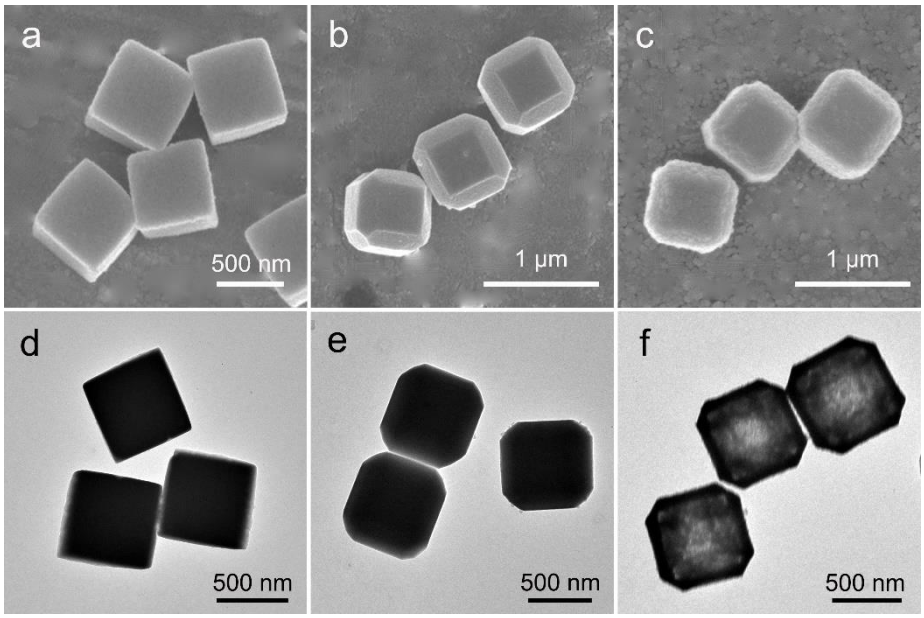

Figure 2. (a-c) FESEM images and (d-f) TEM images of the (a, d) ZIF-67 nanocubes, (b, e) ZIF-67@ZIF-8 polyhedrons, and (c, f) CoS_2@ZnS DSNBs.

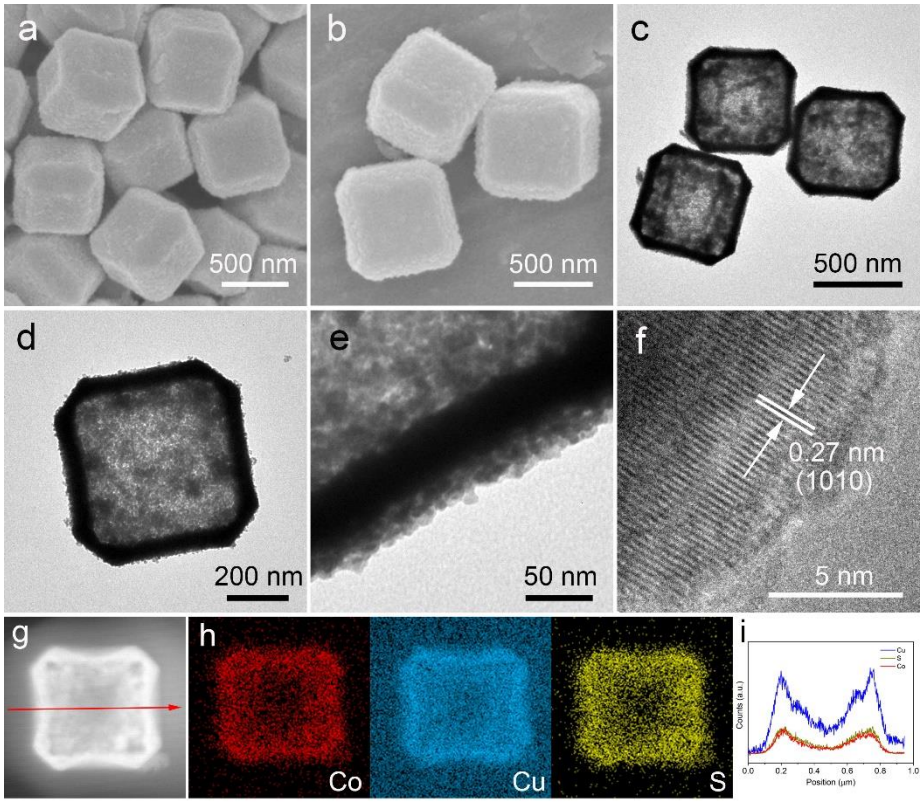

Figure 3. (a, b) FESEM images, (c-e) TEM images, and (f) HRTEM image of Cu-CoS_2@Cu_xS DSNBs. (g) High-angle annular dark-field scanning transmission electron microscopy (HAADF-STEM), and (h) elemental mappings of a single Cu-CoS_2@Cu_xS nanobox, (i) linear elemental distributions of Cu, Co, and S, corresponding to the red arrow in (g), respectively.

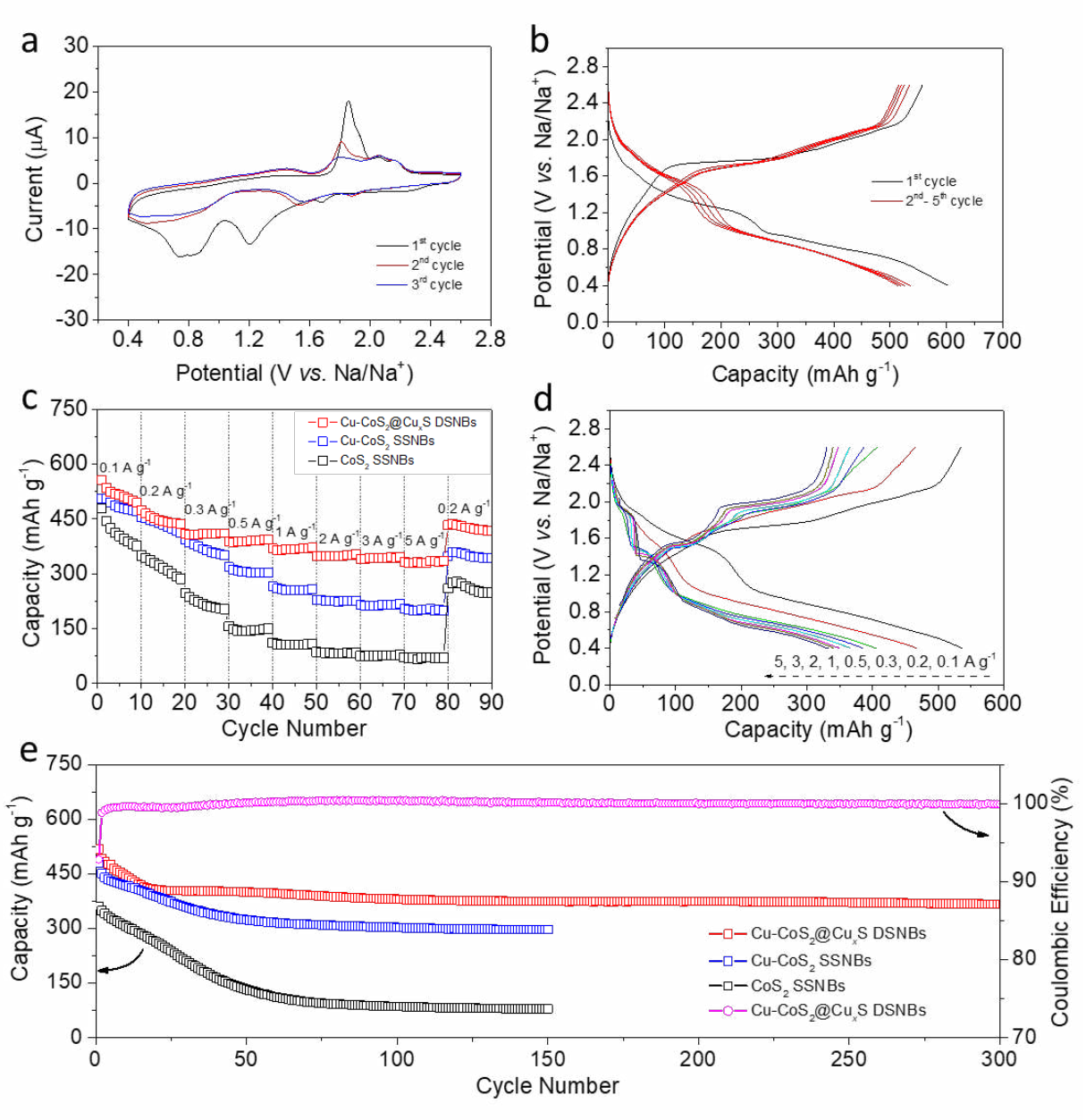

Figure 4. (a) The 1st to 3rd cyclic voltammograms of the Cu-CoS_2@Cu_xS DSNBs electrode at a scan rate of 0.1 mV s^{-1}. (b) Typical discharge-charge curves of the Cu-CoS_2@Cu_xS DSNBs electrode at a current density of 0.1 A g^{-1}. (c) Rate performance of the Cu-CoS_2@Cu_xS DSNBs, Cu-CoS_2 SSNBs, and CoS_2 SSNBs. (d) The corresponding discharge-charge curves of Cu-CoS_2@Cu_xS DSNBs at various current densities. (e) Cycling performance of the Cu-CoS_2@Cu_xS DSNBs, Cu-CoS_2 SSNBs, and CoS_2 SSNBs at a current density of 0.3 A g^{-1}.

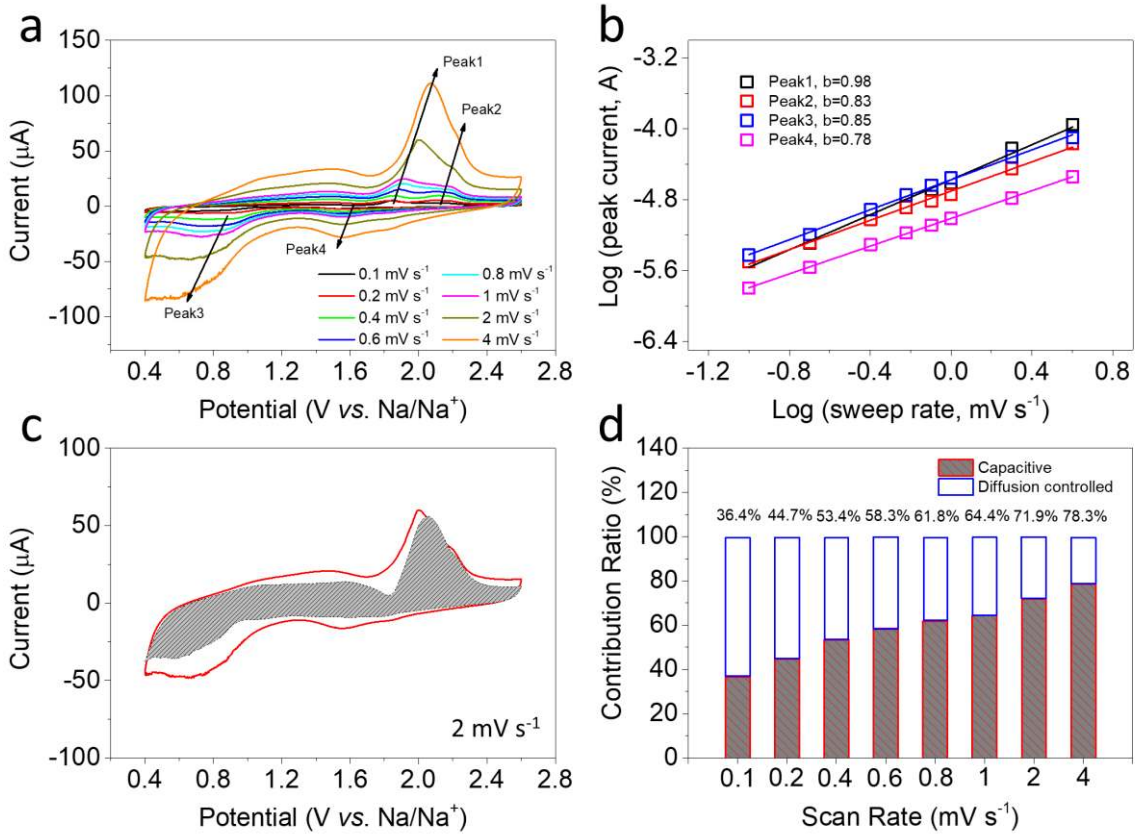

Figure 5. (a) The cyclic voltammograms of the Cu-CoS_2@Cu_xS DSNBs electrode at various scan rates. (b) Determination of the *b* value using the relationship between the peak current and scan rate. (c) Separation of the capacitive and diffusion currents in the cyclic voltammogram of the Cu-CoS_2@Cu_xS DSNBs electrode at a scan rate of 2.0 mV s^{-1} with the capacitive fraction shown by the shaded grey region. (d) Contribution ratio of the capacitive and diffusion-controlled charge versus scan rate.

for Table of Content Entry

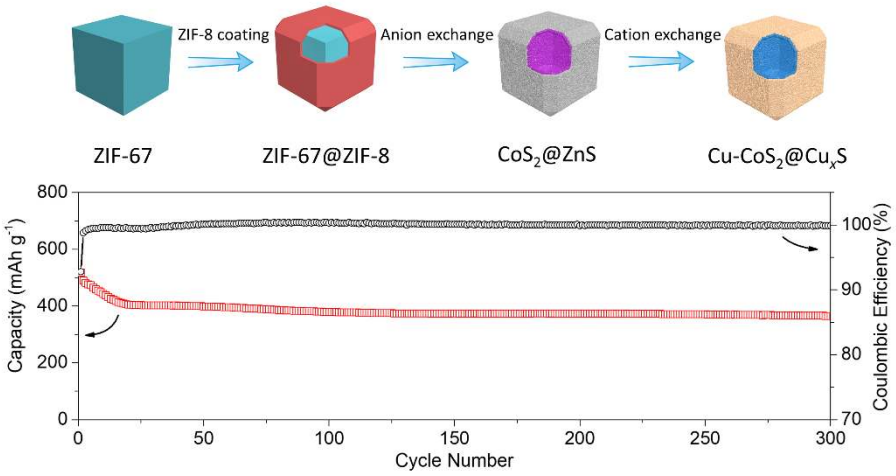

Cu-substituted CoS_2@Cu_xS double-shelled nanoboxes are synthesized through a multistep metal-organic framework (MOF)-based templating strategy. With the unique shell architecture and complex composition, these Cu-substituted CoS_2@Cu_xS double-shelled nanoboxes exhibit enhanced sodium storage performance in terms of high reversible capacity, superior rate capability, and long cycle life.